Revista de Neurología

Rev. Neurol. **2026**; 81(11): 55179
https://doi.org/10.31083/RN55179

Original Article

Topographic Patterns and Etiologic Spectrum of Isolated Pontine Infarcts on Diffusion-Weighted MRI

Musa Muhtaroglu[1,*], Belin Kamiloglu[2], Ferda Selcuk Muhtaroglu[2]

[1]Department of Anatomy, Faculty of Medicine, European University of Lefke, 99010 Lefke, Northern Cyprus, TR-10 Mersin, Turkey
[2]Department of Neurology, Dr. Burhan Nalbantoglu State Hospital, 99010 Nicosia, Northern Cyprus
*Correspondence: mmuhtaroglu@eul.edu.tr (Musa Muhtaroglu)
Academic Editor: Angela Vidal-Jordana
Submitted: 23 June 2026 Revised: 9 October 2026 Accepted: 30 October 2026 Published: 19 November 2026

Abstract

Background: Isolated pontine infarcts vary in location and may reflect different vascular mechanisms. We describe diffusion-weighted imaging (DWI) patterns and examine their distribution across routinely assigned etiologic categories in a hospital-based acute ischemic stroke sample. **Methods:** This retrospective single-center study examined 69 patients with DWI-confirmed acute infarction confined to the pons. Cases were identified from 365 acute ischemic stroke records collected from January 2021 through September 2022. We analyzed the National Institutes of Health Stroke Scale (NIHSS) scores at admission, lesion side, rostrocaudal segment, recorded morphology/topography, vascular risk factors, and Trial of Org 10172 in Acute Stroke Treatment (TOAST)-based etiology. Sparse contingency tables were evaluated with Fisher-Freeman-Halton tests using Monte Carlo estimation, and related comparisons were adjusted with the Holm method. **Results:** Mean age was 68.4 ± 14.0 years, 46 (66.7%) were male, and the median NIHSS at admission was 3 (interquartile range, 2–6). The most frequent features were middle segment (51/69, 73.9%), anteromedial morphology (44/69, 63.8%), and the operational small-vessel/lacunar group (36/69, 52.2%). Global NIHSS comparisons by lesion side and recorded morphology/topography yielded raw p-values of 0.023 and 0.029 (epsilon-squared, 0.084 and 0.118), respectively, with neither remaining significant after adjustment across four NIHSS comparisons (adjusted $p = 0.091$ for both). In the full cohort, etiology was associated with lesion side (adjusted $p < 0.001$; Cramer's V = 0.722) and recorded morphology/topography (adjusted $p < 0.001$; V = 0.572), but not rostrocaudal segment (adjusted $p = 0.441$; V = 0.253). The six bilateral cases were the same six cases classified as large-artery atherosclerosis. After excluding these six cases, neither lesion side (adjusted $p = 0.479$; V = 0.209) nor recorded morphology/topography (adjusted $p = 0.118$; V = 0.321) remained significantly associated with etiology. **Conclusions:** Anteromedial morphology and the operational small-vessel/lacunar group were the most frequent recorded categories. Middle-pontine predominance may partly reflect allocation of remainder slices to the middle segment. Full-cohort associations of lesion side and recorded morphology/topography with etiology were no longer statistically significant after excluding the six overlapping bilateral/large-artery atherosclerosis cases. Prospective studies should assess topographic dimensions and vascular mechanisms separately using standardized anatomical definitions, quantitative lesion assessment, and parent-artery imaging.

Keywords: brain stem infarctions; pons; diffusion magnetic resonance imaging; stroke; retrospective studies

1. Introduction

Pontine infarcts are an important subgroup of posterior-circulation ischemic stroke, with their clinical features often dependent on the precise location of the lesion. Within a compact region, the pons contains the corticospinal and corticobulbar tracts, medial lemniscus pathways, pontine nuclei, cerebellar connections, vestibulo-ocular networks, and cranial nerve nuclei. Even a small infarct can therefore produce a varied clinical picture. Magnetic resonance imaging (MRI)-based studies have likewise shown that isolated pontine infarction encompasses several anatomical and clinical patterns rather than a single uniform syndrome [1,2].

The location of a pontine lesion can help to explain its clinical presentation. Paramedian and anteromedial lesions may affect the descending corticospinal tracts and produce motor deficits, whereas tegmental or lateral lesions may be associated with sensory, cerebellar, oculomotor, or other cranial nerve findings. Early studies of paramedian pontine infarction and named pontine syndromes established the basis for interpreting these clinical-anatomical relationships on MRI [1,2,3].

Several vascular mechanisms can produce a pontine infarct, including small-vessel arteriopathy, lipohyalinosis, branch atheromatous disease, and parent-artery atherosclerotic plaque involving perforator origins. Fisher's pathological account of lacunes and Caplan's description of intracranial branch atheromatous disease remain central to this distinction [4,5]. Moreover, clinical series have used lesion configuration and vascular findings to distinguish the mechanisms [6,7].

High-resolution vessel-wall MRI has refined the etiologic assessment of isolated pontine infarction. Early studies detected basilar artery plaques in patients with parame-

Copyright: © 2026 The Author(s). Published by IMR Press.
This is an open access article under the CC BY 4.0 license.

Publisher's Note: IMR Press stays neutral with regard to jurisdictional claims in published maps and institutional affiliations.

dian or medial pontine infarcts, despite the absence of substantial luminal stenosis on conventional angiography [8,9]. Subsequent studies related plaque distribution and vascular geometry to pontine lesion patterns [10,11]. Consequently, lumen-based imaging may fail to detect parent-artery disease in selected cases. In routine retrospective cohorts, vessel-wall MRI may not be uniformly available, and etiologic classification is therefore dependent on the investigations conducted during care and on standard stroke-subtype systems.

Lesion topography and morphology have been examined in relation to progressive motor deficits [12,13,14]. Other cohorts have evaluated clinical- and lesion-based correlates of early neurological deterioration [15,16,17]. Small-vessel-disease burden and other imaging biomarkers have also been examined [18]. While these dimensions are often reported separately, the present study evaluated the available vascular risk factors, lesion side, rostrocaudal segment, recorded morphology/topography, admission stroke severity, and etiologic category within a single hospital-based cohort.

We aimed to characterize the diffusion-weighted imaging (DWI)-defined topographic distribution and Trial of Org 10172 in Acute Stroke Treatment (TOAST)-based etiologic spectrum of isolated pontine infarction in a single-center cohort. We further examined topography-etiology relationships and compared National Institutes of Health Stroke Scale (NIHSS) severity at admission across lesion side, rostrocaudal segment, recorded morphology/topography, and etiologic category.

2. Materials and Methods

2.1 Study Design and Setting

This retrospective, single-center observational study was conducted using routinely collected data from patients assessed for acute ischemic stroke in the Neurology Department of Dr. Burhan Nalbantoğlu State Hospital between January 2021 and September 2022. The report follows the Strengthening the Reporting of Observational Studies in Epidemiology (STROBE) recommendations, and the complete checklist is provided as **Supplementary Material-STROBE Checklist** [19].

The departmental dataset comprised 365 acute ischemic stroke records from the study period. The retained dataset did not include a patient-level screening log or document consecutive enrollment. Accordingly, 69/365 is reported only as a descriptive record-based hospital proportion, rather than population incidence or prevalence. No confidence interval is presented because a binomial interval would not capture uncertainty in case ascertainment and record selection. No a priori sample-size calculation was performed, and the analytic sample comprised the 69 patients whose records satisfied the defined imaging eligibility criteria.

2.2 Participants and Eligibility Criteria

Patients were eligible when DWI demonstrated an acute ischemic lesion confined to the pons, without a concurrent acute supratentorial, cerebellar, medullary, or mesencephalic infarct. Remote chronic infarcts were permitted. The 12 records containing an accompanying-infarct flag referred exclusively to remote chronic lesions, and none contained a concurrent acute non-pontine infarct. Acute lesion isolation was established from the contemporaneous DWI/apparent diffusion coefficient (ADC) findings and the clinical imaging record. Each included record represented a unique patient, and the de-identified analysis file contained no direct personal identifiers.

2.3 Clinical Variables and Vascular Risk Factors

Age and sex were recorded as demographic variables. At the initial presentation in the emergency department, each patient's neurological status was assessed by a neurologist using the NIHSS [20]. The first documented admission NIHSS score was retrospectively retrieved from routine clinical records. Because the exact interval between symptom onset and NIHSS assessment was unavailable, the scores were interpreted as measures of neurological severity at presentation rather than as measurements obtained at a uniform time point after symptom onset. Recorded vascular risk variables included hypertension, diabetes mellitus, hyperlipidemia, smoking history, coronary artery disease, prior cerebrovascular event, and atrial fibrillation.

All seven vascular risk variables were available as patient-level binary data. They were analyzed as recorded, and not subsequently redefined by laboratory values and medication histories. Six variables other than atrial fibrillation were included in the secondary risk-factor-by-etiology analyses. Atrial fibrillation was retained descriptively because it contributed directly to cardioembolic classification. The analysis file contained no missing values for the variables used, and thus all analyses included 69 patients without imputation. Exact symptom-onset-to-MRI intervals and modified Rankin Scale data were unavailable.

Vascular risk factor data were retrospectively extracted from hospital discharge summaries. Hypertension, diabetes mellitus, hyperlipidemia, and coronary artery disease were identified from the corresponding clinical diagnoses documented in these summaries. Smoking history referred specifically to documented active smoking. Prior cerebrovascular events were identified from the recorded history of cerebrovascular events preceding the index stroke. Atrial fibrillation was identified from its documentation in the discharge summaries. Each variable was analyzed using its existing patient-level binary coding. The recorded classifications were retained without retrospective redefinition using laboratory values or medication histories.

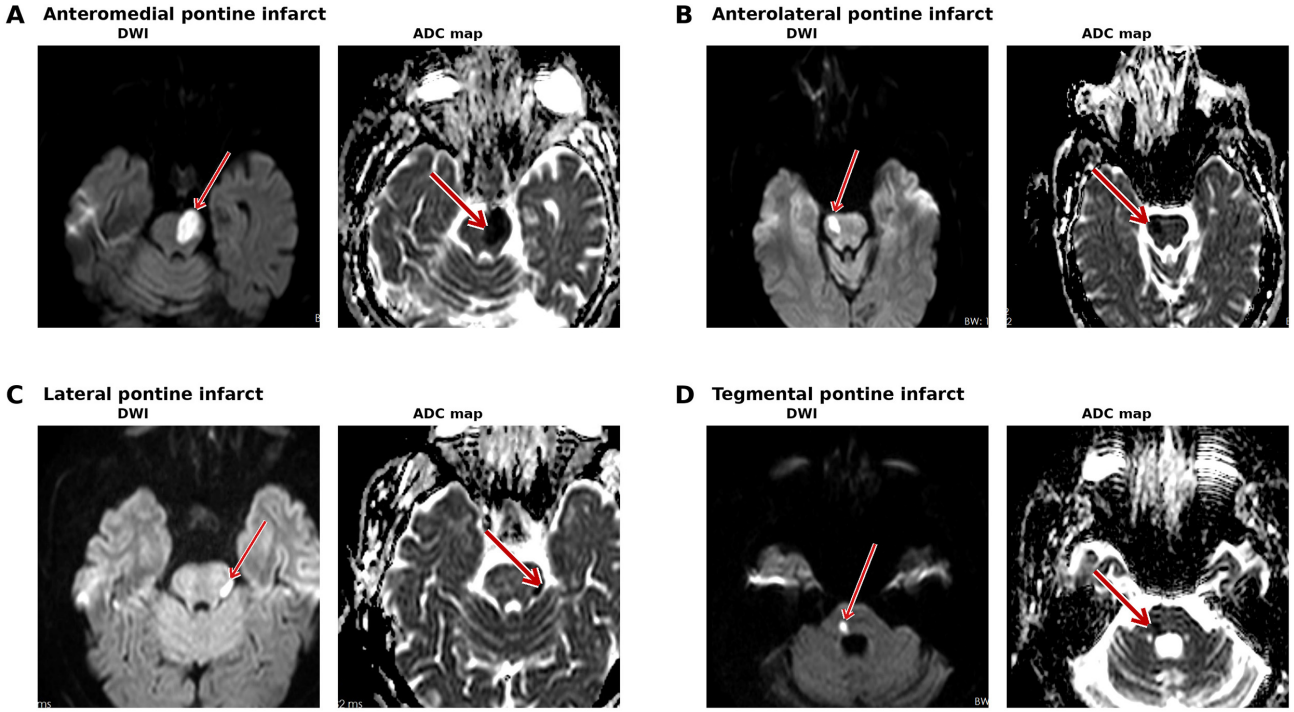


Fig. 1. Representative axial DWI and corresponding ADC maps illustrating the recorded anatomical patterns: (A) anteromedial, (B) anterolateral, (C) lateral, and (D) tegmental pontine infarction. Red arrows identify the DWI-hyperintense lesions and corresponding ADC-hypointense areas. DWI, diffusion-weighted imaging; ADC, apparent diffusion coefficient.

2.4 Neuroimaging and Topographic Classification

Isolated pontine infarction was identified on axial DWI and the corresponding ADC map. Representative console exports that could be recovered were acquired on a 1.5-T Achieva MRI system (Philips Medical Systems Nederland B.V., Best, North Brabant, the Netherlands). The verified export-level parameters were a 90-degree flip angle, repetition times of approximately 3715–6504 ms, echo times of approximately 100.7–142.5 ms, acquisition matrices from 105 × 152 to 128 × 172, one to three signal averages, SENSE head or head/neck receiver coils, a 5.0-mm slice thickness, and diffusion/ADC reconstruction documented at b = 1000 s/mm^2. ADC maps were generated at the scanner console. Complete Digital Imaging and Communications in Medicine (DICOM) protocols and full multi-b-value series were not retained for all 69 examinations. Therefore, these values describe the recoverable representative exports rather than a uniform cohort-wide protocol.

Two neurologists with 16 and 6 years of clinical experience independently reviewed all MRI examinations retrospectively. Each reader was blinded to the patients' clinical, laboratory, and etiologic classification data and to the other reader's assessment. Disagreements regarding lesion presence or location were resolved by consensus. Because the dataset retained the consensus classifications but not the paired pre-consensus ratings, inter-rater agreement could not be calculated retrospectively. Lesion side (right, left, or bilateral) and rostrocaudal segment (upper, middle, or lower pons) were analyzed separately. A legacy, mutually exclusive morphology/topography variable was used to classify lesions as anteromedial, lateral, bilateral, unilateral multiple, anterolateral, or tegmental. Coordinate-based boundaries for these labels and separate territory labels for bilateral and multiple lesions were not retained. Accordingly, they were used as recorded clinical categories rather than as coordinate-defined arterial territories in the analyses. Lesion volume, maximum diameter, basal-surface extension, and other quantitative measures of lesion burden were unavailable.

For each examination, axial MRI slices containing pontine parenchyma were counted and divided craniocaudally into upper, middle, and lower thirds, with sagittal images used for anatomical guidance. When the number of slices was not divisible by three, the remaining one or two slices were allocated to the middle third. This allocation systematically enlarges the middle category in examinations with remainder slices and may increase the proportion assigned to it. The retained dataset contained one segment label per patient; no separate assignment rule was applied to lesions crossing a boundary. The recorded segment was therefore analyzed as an operational topographic category rather than as a standardized physical measure of rostrocaudal lesion extent. Representative DWI/ADC pairs illustrate the anatomical patterns in Fig. 1, and laterality/multiplicity in Fig. 2.

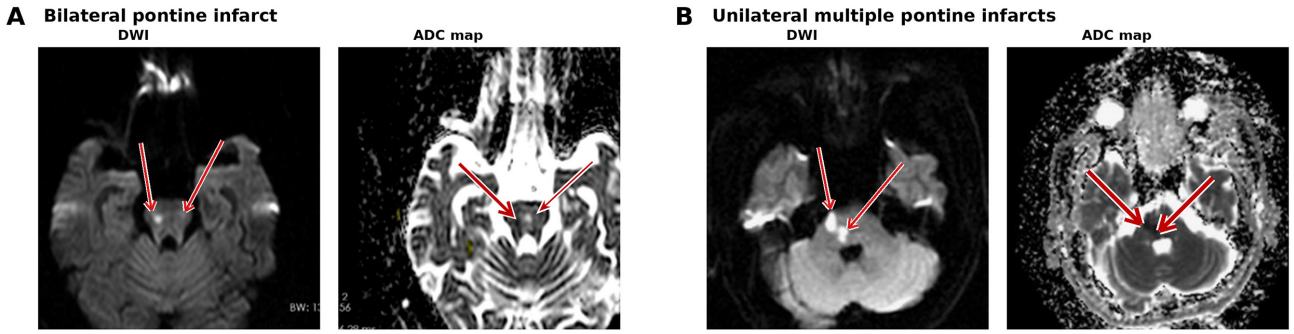


Fig. 2. Representative axial DWI and corresponding ADC maps illustrating laterality and multiplicity: (A) bilateral pontine infarction and (B) unilateral multiple pontine infarcts. Red arrows identify the DWI-hyperintense lesion components; arrows on the ADC maps indicate corresponding areas of reduced diffusivity.

Two neurologists selected the representative DWI and ADC images and confirmed the location of the annotations. The original 600-dpi TIFF files were cropped to reduce console information, and panel dimensions and labels were standardized. Image intensity and lesion signal were not altered. Because complete DICOM series were unavailable, NIfTI conversion and volumetric segmentation could not be performed.

2.5 Etiologic Evaluation and Classification

The treating neurologists assigned the original etiologic categories during routine clinical care and documented them in the discharge records, drawing on the vascular, cardiac, rhythm, laboratory, and other investigations performed. For the analysis, five TOAST-based categories were used: operational small-vessel/lacunar group, cryptogenic stroke, stroke of other determined etiology, cardioembolic stroke, and large-artery atherosclerosis [21]. Because no study-specific blinded panel readjudicated the full cohort, these categories represent an operational classification based on routine records. Classification was not blinded to lesion topography, and the available records did not permit reconstruction of a uniform stenosis threshold or a patient-level completion matrix for every etiologic investigation. Two neurologists (FSM, BK) reviewed nine records carrying specific or potentially ambiguous etiologic labels and reached consensus on their analytic categories, with seven being classified in the "other-determined" group. The record labeled as branch atheromatous disease and the record with an isolated acute-phase Protein S deficiency result were retained in the original operational small-vessel/lacunar group by neurologist consensus, without asserting a confirmed intrinsic small-vessel mechanism. Their influence on the findings was assessed in additional post hoc sensitivity analyses excluding both records (**Supplementary Table 1**).

High-resolution vessel-wall MRI and standardized long-term rhythm monitoring were not performed uniformly. This variability can introduce potential etiologic misclassification, particularly among small-vessel disease, branch atheromatous disease, nonstenotic parent-artery plaque, large-artery atherosclerosis, and cryptogenic stroke.

2.6 Statistical Analysis

Continuous variables are presented as the mean ± standard deviation, and as the median with interquartile range. Categorical variables are reported as counts and percentages. For groups of two patients, individual NIHSS values were reported rather than estimated quartiles. The primary analysis was the descriptive characterization of 69 isolated pontine infarcts. Cross-tabulations and NIHSS subgroup comparisons were secondary and exploratory.

We compared NIHSS distributions across lesion side, rostrocaudal segment, recorded morphology/topography, and etiologic category using tie-corrected Kruskal-Wallis tests. *p*-values for the four global comparisons were adjusted using the Holm method. Epsilon-squared was calculated as $\varepsilon^2 = \max[0, (H - k + 1)/(n - k)]$, where H is the Kruskal-Wallis statistic, k is the number of groups, and n is the total sample size; negative estimates were set to zero. Exploratory pairwise comparisons were performed using two-sided permutation-based Mann-Whitney U tests with 200,000 resamples. Within each domain, *p*-values were adjusted using the Holm method, and rank-biserial correlations were reported as descriptive effect estimates. Bootstrap confidence intervals are not reported because resampling very small groups can produce unstable or degenerate intervals. Fixed random seeds were used for reproducibility. Sparse topography-by-etiology and risk-factor-by-etiology tables were analyzed using Monte Carlo estimates of Fisher-Freeman-Halton exact *p*-values (500,000 resamples; fixed seed 55179), with Cramer's V as the effect-size measure. Holm adjustment was applied separately to the three topography-by-etiology tests and the six risk-factor-by-etiology tests. Atrial fibrillation was excluded from risk-factor-by-etiology testing because it contributed directly to cardioembolic classification. To assess the influence of the complete overlap between bilateral

Table 1. Baseline clinical and demographic characteristics of the study population.

Characteristic	Overall (n = 69)	Notes
Study population	69	DWI-MRI-defined isolated pontine infarct cases included in the analysis
Record-based hospital proportion	69/365 (18.9%)	365 departmental stroke records; not population incidence or prevalence
Age, years	68.4 ± 14.0	Median 70 (IQR 59–79); range 28–100
Male	46 (66.7)	
Female	23 (33.3)	
Admission NIHSS score	4.8 ± 4.7	Median 3 (IQR 2–6); range 0–17
Hypertension	36 (52.2)	
Diabetes mellitus	33 (47.8)	
Hyperlipidemia	31 (44.9)	Patient-level binary variable; included in secondary etiology analysis
Smoking history	34 (49.3)	Patient-level binary variable; included in secondary etiology analysis
Coronary artery disease	17 (24.6)	
Prior cerebrovascular event	14 (20.3)	
Atrial fibrillation	7 (10.1)	

Values are presented as the mean ± SD or n (%), unless otherwise indicated. IQR, interquartile range; MRI, magnetic resonance imaging; NIHSS, National Institutes of Health Stroke Scale; SD, standard deviation.

involvement and large-artery atherosclerosis, the side-by-etiology and recorded morphology/topography-by-etiology analyses were repeated after excluding those six patients. The two *p*-values for sensitivity were adjusted together using the Holm method. A raw two-sided $p < 0.05$ served only as an exploratory screening threshold, and inference was based on adjusted results. All reported calculations were reproduced using Python 3.12.14 (Python Software Foundation; https://www.python.org/), with SciPy version 1.17.0 (SciPy developers; https://scipy.org/) and NumPy version 2.3.5 (NumPy developers; https://numpy.org/).

An additional post hoc sensitivity analysis excluded the two records described in Section 2.5, leaving 67 patients. Topography-by-etiology associations, global NIHSS comparisons, and risk-factor-by-etiology associations were re-evaluated using the corresponding primary-analysis methods. Holm adjustment was applied separately to the three topography tests, four global NIHSS comparisons, and six risk-factor tests. No additional pairwise comparisons were performed. A further analysis additionally excluded the six overlapping bilateral/large-artery atherosclerosis cases, leaving 61 patients; the lesion-side and recorded morphology/topography tests were adjusted together using the Holm method. The original 69-patient primary analysis was retained unchanged.

3. Results

3.1 Study Population and Baseline Characteristics

Among the 365 records for acute ischemic stroke in the departmental dataset, 69 met the imaging definition of isolated pontine infarction, representing 69 patients in the analytic sample. The descriptive record-based hospital proportion was 18.9% (69/365). The denominator is the center's departmental record set for the study period, not a population at risk or a confirmed, consecutively enrolled cohort.

The mean age was 68.4 ± 14.0 years, with a median of 70 years (interquartile range (IQR), 59–79; range, 28–100). Forty-six patients (66.7%) were male. The mean NIHSS score at admission was 4.8 ± 4.7, with a median of 3 (IQR, 2–6; range, 0–17) (Table 1).

Hypertension was present in 36 patients (52.2%), diabetes mellitus in 33 (47.8%), hyperlipidemia in 31 (44.9%), smoking history in 34 (49.3%), coronary artery disease in 17 (24.6%), prior cerebrovascular event in 14 (20.3%), and atrial fibrillation in 7 (10.1%).

3.2 MRI-Defined Topographic and Etiologic Distribution

Lesions were right-sided in 34 patients (49.3%), left-sided in 29 (42.0%), and bilateral in 6 (8.7%). The middle segment was the most frequently recorded rostrocaudal category (51/69, 73.9%), with the upper and lower segments each containing 9 patients (13.0%).

Anteromedial was the most common recorded morphology/topography category (44/69, 63.8%), followed by lateral (11/69, 15.9%). Each remaining category contained two to six patients (Table 2). Because this legacy variable combines anatomical pattern with laterality and multiplicity, its categories do not represent separate arterial territories.

The operational small-vessel/lacunar group was the most common etiologic category (36/69, 52.2%). The distributions of cryptogenic, other-determined, cardioembolic, and large-artery categories are presented in Table 2.

The other-determined group comprised seven patients, with one patient assigned each of the following diagnoses: basilar artery dolichoectasia, vertebrobasilar dolichoectasia, polycythemia vera-associated hyperviscosity, vertebral artery dissection, giant cell arteritis, Behçet disease with recorded neurological involvement, and basilar artery dissection. Two additional records carried specific labels: one referred to branch atheromatous disease and the other to an

Table 2. Diffusion-weighted MRI-defined topographic and etiologic distribution of isolated pontine infarcts.

Domain	Category	n	%
Lesion side	Right	34	49.3
Lesion side	Left	29	42.0
Lesion side	Bilateral	6	8.7
Rostrocaudal segment	Upper pons	9	13.0
Rostrocaudal segment	Middle pons	51	73.9
Rostrocaudal segment	Lower pons	9	13.0
Recorded morphology/topography	Anteromedial	44	63.8
Recorded morphology/topography	Lateral	11	15.9
Recorded morphology/topography	Bilateral	6	8.7
Recorded morphology/topography	Unilateral multiple	4	5.8
Recorded morphology/topography	Anterolateral	2	2.9
Recorded morphology/topography	Tegmental	2	2.9
Etiologic classification	Operational small-vessel/lacunar	36	52.2
Etiologic classification	Cryptogenic stroke	13	18.8
Etiologic classification	Other determined etiology	7	10.1
Etiologic classification	Cardioembolic stroke	7	10.1
Etiologic classification	Large-artery atherosclerosis	6	8.7

Percentages use n = 69 as the denominator and may not total 100 because of rounding. The recorded morphology/topography variable is a legacy mutually exclusive field that combines territory, laterality, and multiplicity. Etiologic categories follow the Trial of Org 10172 in Acute Stroke Treatment (TOAST)-based operational classification described in Section 2.5.

isolated acute-phase Protein S deficiency. Following consensus by the neurologists, both were classified in the operational small-vessel/lacunar group and were not regarded as confirmed alternative causal mechanisms.

3.3 Admission NIHSS Severity According to Topography and Etiology

The distribution of admission NIHSS scores differed in the unadjusted global analyses according to lesion side ($H = 7.576$; $p = 0.023$; epsilon-squared = 0.084) and recorded morphology/topography ($H = 12.443$; $p = 0.029$; epsilon-squared = 0.118). After adjustment across the four global NIHSS comparisons, neither of these comparisons remained significant (Holm-adjusted $p = 0.091$ for both). NIHSS distributions did not differ by rostrocaudal segment ($H = 0.241$; raw and adjusted $p = 0.887$) or etiologic category ($H = 6.806$; raw $p = 0.147$; adjusted $p = 0.293$) (Table 3).

No global NIHSS comparison remained significant after Holm adjustment. Exploratory pairwise results are retained in **Supplementary Table 2** for completeness, with group sizes, permutation *p*-values, Holm-adjusted *p*-values, and descriptive rank-biserial correlations. Bootstrap confidence intervals are omitted. Pairwise contrasts do not supersede the multiplicity-adjusted omnibus results, particularly when groups contain only two to four patients.

3.4 Topography-Etiology Cross-Tabulation and Secondary Risk-Factor Analyses

In the full cohort, Monte Carlo tests showed evidence of associations between etiologic category and lesion side (raw and Holm-adjusted $p < 0.001$; Cramer's V = 0.722), and between etiologic category and recorded morphology/topography (raw and adjusted $p < 0.001$; Cramer's V = 0.572), but not between etiologic category and rostrocaudal segment (raw and adjusted $p = 0.441$; Cramer's V = 0.253) (Table 4). All six bilateral cases were classified as large-artery atherosclerosis, and no unilateral case was assigned to that etiologic category. This complete overlap was therefore embedded in the side-by-etiology table. Because bilateral involvement was also a category of the legacy variable, it too was embedded in the morphology/topography-by-etiology table. Other cell distributions, including the classification of all 11 lateral cases as operational small-vessel/lacunar group, also contributed to the full-cohort statistics. In post hoc sensitivity analyses that excluded the six overlapping bilateral/large-artery atherosclerosis cases, neither the side-by-etiology association (n = 63; raw and Holm-adjusted $p = 0.479$; Cramer's V = 0.209) nor the association between recorded morphology/topography and etiology (n = 63; raw $p = 0.059$; Holm-adjusted $p = 0.118$; Cramer's V = 0.321) remained statistically significant after Holm adjustment across the two sensitivity tests. Thus, the full-cohort associations were no longer statistically significant after exclusion of the six overlapping cases. These sensitivity analyses do not establish the absence of an association.

After excluding the two records with uncertain etiologic assignments (n = 67), associations of etiology with lesion side and recorded morphology/topography remained significant (both Holm-adjusted $p < 0.001$; Cramer's V = 0.721 and 0.577, respectively), whereas the association

Table 3. Admission NIHSS severity according to topographic and etiologic subgroups.

Domain	Subgroup	n	NIHSS median (IQR) or individual values	Raw global *p*-value	Holm-adjusted *p*-value
Lesion side	Right	34	3 (1.25–4)	0.023	0.091
	Left	29	4 (2–5)		
	Bilateral	6	14.5 (12.5–16.5)		
Rostrocaudal segment	Upper pons	9	4 (2–5)	0.887	0.887
	Middle pons	51	3 (2–6)		
	Lower pons	9	4 (3–6)		
Recorded morphology/ topography	Anteromedial	44	3 (1–5)	0.029	0.091
	Lateral	11	4 (3–4.5)		
	Bilateral	6	14.5 (12.5–16.5)		
	Unilateral multiple	4	1.5 (0–3)		
	Anterolateral	2	2, 6		
	Tegmental	2	4, 7		
Etiologic category	Operational small-vessel/lacunar	36	3 (1.75–4.25)	0.147	0.293
	Cryptogenic	13	3 (2–4)		
	Other determined	7	3 (2–5.5)		
	Cardioembolic	7	4 (2–5)		
	Large-artery atherosclerosis	6	14.5 (12.5–16.5)		

Global comparisons used tie-corrected Kruskal-Wallis tests. Holm adjustment was applied across the four global NIHSS comparisons. Epsilon-squared was calculated as $\varepsilon^2 = \max[0, (H - k + 1)/(n - k)]$; negative estimates were set to zero. Values were 0.084 for lesion side, 0.000 for segment, 0.118 for recorded morphology/topography, and 0.044 for etiology. Individual NIHSS values are shown for groups with n = 2. All analyses are exploratory.

Table 4. Cross-tabulation of available topographic variables and etiologic categories.

Domain	Category	SVO	Cryptogenic	Other	Cardioembolic	LAA	Raw Monte Carlo *p* (Holm-adjusted *p*); V
Side	Right	21	8	2	3	0	<0.001 (<0.001); 0.722
	Left	15	5	5	4	0	
	Bilateral	0	0	0	0	6	
Segment	Upper	7	0	1	1	0	0.441 (0.441); 0.253
	Middle	22	12	6	5	6	
	Lower	7	1	0	1	0	
Recorded morphology/ topography	Anteromedial	19	13	7	5	0	<0.001 (<0.001); 0.572
	Lateral	11	0	0	0	0	
	Bilateral	0	0	0	0	6	
	Unilateral multiple	3	0	0	1	0	
	Anterolateral	2	0	0	0	0	
	Tegmental	1	0	0	1	0	
Total		36	13	7	7	6	

Counts represent patients. Raw *p*-values are Fisher-Freeman-Halton Monte Carlo estimates based on 500,000 resamples (fixed seed 55179); adjusted *p*-values were obtained with the Holm method across the three topography-by-etiology tests. V denotes Cramer's V. Small vessel occlusion (SVO), operational small-vessel/lacunar group (legacy abbreviation); LAA, large-artery atherosclerosis. All six bilateral cases were classified as LAA, and no unilateral case was classified as LAA. This complete overlap also affects interpretation of the recorded morphology/topography association, because bilateral involvement is one of the categories of that legacy variable. The full-cohort statistics also reflect other cell distributions, including the classification of all 11 lateral cases as SVO.

with rostrocaudal segment remained nonsignificant (adjusted $p = 0.357$). Global NIHSS comparisons and vascular risk-factor associations remained nonsignificant after adjustment. After additionally excluding the six overlapping bilateral/large-artery atherosclerosis cases (n = 61), neither lesion side nor recorded morphology/topography was significantly associated with etiology after Holm adjustment (adjusted $p = 0.536$ and 0.076, respectively). Thus, the principal adjusted inferences were consistent with the primary analyses. These sensitivity results assess the influence of

Table 5. Vascular risk factors stratified by etiologic category.

Risk factor	Operational small-vessel/lacunar (n = 36)	Cryptogenic (n = 13)	Other determined (n = 7)	Cardioembolic (n = 7)	Large-artery atherosclerosis (n = 6)	Raw Monte Carlo *p* (Holm-adjusted *p*); V
Hypertension	17 (47.2)	8 (61.5)	4 (57.1)	3 (42.9)	4 (66.7)	0.824 (1.000); 0.154
Diabetes mellitus	16 (44.4)	5 (38.5)	5 (71.4)	3 (42.9)	4 (66.7)	0.562 (1.000); 0.212
Hyperlipidemia	18 (50.0)	6 (46.2)	2 (28.6)	3 (42.9)	2 (33.3)	0.856 (1.000); 0.146
Smoking history	16 (44.4)	9 (69.2)	3 (42.9)	3 (42.9)	3 (50.0)	0.617 (1.000); 0.196
Coronary artery disease	11 (30.6)	0 (0.0)	4 (57.1)	1 (14.3)	1 (16.7)	0.031 (0.189); 0.371
Prior cerebrovascular event	6 (16.7)	0 (0.0)	3 (42.9)	3 (42.9)	2 (33.3)	0.033 (0.189); 0.354
Atrial fibrillation	0 (0.0)	0 (0.0)	0 (0.0)	7 (100.0)	0 (0.0)	Not tested

Values are presented as n (percentage within the etiologic subtype). Risk factors were not mutually exclusive. Fisher-Freeman-Halton Monte Carlo *p*-values and Cramer's V are reported for six patient-level risk factors; Holm adjustment was applied across these six tests. Atrial fibrillation was not tested because it contributed directly to the cardioembolic classification. All analyses are exploratory.

the two assignments; they do not validate their etiologic classification (**Supplementary Table 1**).

None of the six patient-level vascular risk factors were associated with etiologic category after Holm adjustment. Only coronary artery disease (raw $p = 0.031$; adjusted $p = 0.189$; Cramer's V = 0.371) and prior cerebrovascular event (raw $p = 0.033$; adjusted $p = 0.189$; Cramer's V = 0.354) crossed the unadjusted screening threshold. Hypertension, diabetes mellitus, hyperlipidemia, and smoking history each had raw p-values > 0.05. Atrial fibrillation is presented descriptively in Table 5.

4. Discussion

In this hospital cohort of acute ischemic stroke, the middle segment and recorded anteromedial morphology were the most frequent topographic categories, while the operational small-vessel/lacunar group was the leading routine etiologic classification. Full-cohort analyses showed clustering of the etiology with lesion side and recorded morphology/topography. However, neither association remained statistically significant following exclusion of the six cases shared by the bilateral and large-artery atherosclerosis categories. No statistically significant association was detected between rostrocaudal level and etiologic category. Admission NIHSS varied descriptively across groups, but no global comparison remained significant after multiplicity adjustment. Together, our findings characterize the anatomical-etiologic profile of this cohort, while showing that laterality, morphology, and mechanism require separate evaluation.

Classic clinical-MRI series have previously described isolated pontine infarction using paramedian, lateral, tegmental, and basal or ventral patterns [1,2,3]. Later etiopathogenic and follow-up studies reinforced the notion that isolated pontine infarction is mechanistically heterogeneous rather than a uniform lacunar entity [6,7]. Recent cohorts have related early neurological deterioration to the measured lesion size and ventral-surface extension [22,23,24], while a systematic review emphasized heterogeneity in the definitions and mechanisms of deterioration in lacunar ischemic stroke [25]. Anteromedial lesions accounted for 63.8% of the present cohort, which is directionally similar to the 73% reported in a DWI cohort of 205 patients that used a four-territory classification system [26]. This directional similarity is anatomically plausible, but differences in definitions, imaging protocols, and sampling frameworks preclude direct numerical comparison. Because our legacy anteromedial label lacked coordinate-based boundaries, lesion-volume measurements, and a separate basal-surface variable, it is best interpreted as a descriptive clinical-data category rather than as a quantitative arterial-territory or severity measure.

Rostrocaudal level contributed a different finding: the middle pons was the most frequently recorded segment, yet its distribution did not vary significantly across etiologic categories. Previous isolated pontine studies linked topographic location to progressive motor deficits or neurological deterioration [12,13,14], whereas the present analysis examined its relationship with etiologic category. These results are complementary, since a location may be clinically relevant without reliably distinguishing mechanism. Differences in eligibility, segmentation, and image resolution also limit comparison among isolated pontine series [2,12,13], while broader brainstem and unisolated pontine cohorts include different lesion populations [27,28]. Allocating remainder slices to the middle third widened that category in examinations with remainder slices and may have contributed to its high recorded frequency. No separate rule was applied to lesions crossing segment boundaries. The observed middle-pons predominance should therefore be interpreted as a finding under this operational segmentation method, rather than evidence of preferential involvement of anatomically equal thirds. The contribution of the allocation rule cannot be quantified from the retained segment labels.

The topography-by-etiology findings of the full cohort require interpretation in light of the data structure. The same six patients formed both the bilateral group and the entire large-artery atherosclerosis group. Bilateral involvement was also embedded in the legacy morphology variable, and all 11 lateral lesions were classified as operational small-vessel/lacunar group. After exclusion of the six overlapping bilateral/large-artery cases, the side-by-etiology result was nonsignificant, and the recorded morphology/topography result was not statistically significant according to the Holm-adjusted p-value. Because routine etiologic classification was not performed independently of lesion topography, imaging features may also have influenced etiologic assignment. Therefore, the full-cohort p-values and Cramer's V values quantify clustering within this dataset and should not be interpreted as independent anatomical effects. These patterns can be tested in larger studies that record laterality, multiplicity, arterial territory, lesion burden, and parent-artery abnormalities separately, and that assess etiology independently of the imaging labels under study.

The operational small-vessel/lacunar group was the most frequent routine classification. This operational category includes the record labeled branch atheromatous disease and the record with an isolated acute-phase Protein S abnormality. Its frequency does not establish a homogeneous small-vessel mechanism. Intrinsic small-vessel disease, branch atheromatous disease, and parent-artery pathology remain distinct clinical possibilities within this record-based group. Earlier isolated pontine series likewise supported a mixture of penetrating-artery and parent-artery mechanisms [6,7]. Pathological frameworks distinguish lipohyalinotic lacunes from branch atheromatous disease [4,5,29], while high-resolution MRI studies have demonstrated nonstenotic basilar plaque [8,9] and reported associations between plaque features and pontine infarct patterns [10,11,30]. More recent studies have further implicated culprit parent-artery plaques and basilar artery wall pathology that may not be apparent on routine luminal imaging [31,32]. Together, these observations explain why a normal or minimally stenotic lumen does not exclude a parent-artery mechanism. Because vascular imaging and vessel-wall assessment were not uniform, the operational TOAST-based categories derived from routine records remain susceptible to misclassification.

The NIHSS analysis provides complementary clinical context. While the admission severity varied descriptively across lesion groups, none of the global comparisons remained significant after Holm adjustment. Previous studies primarily examined early neurological deterioration rather than a single admission score, and reported associations with topography, etiologic subtype, or vascular imaging features [13,14,15,18,30,33]. The endpoints were therefore different from those of the current study. Patients with bilateral lesions had higher NIHSS ranks, although the complete overlap with large-artery atherosclerosis and the absence of quantitative lesion-burden data preclude attribution to laterality alone. Moreover, conventional NIHSS can underestimate posterior-circulation stroke severity due to the incomplete representation of clinically important features such as dysphagia and gait or truncal ataxia [34]. Serial neurological assessments and functional outcomes are needed to determine how pontine anatomical patterns relate to deterioration and recovery [25,35].

Risk-factor analyses likewise yielded no associations after multiplicity adjustment. Coronary artery disease and prior cerebrovascular events crossed the unadjusted screening threshold but not the adjusted threshold. These factors may warrant further assessment in adequately powered cohorts. Small and uneven subtype cells precluded reliable multivariable modeling. Consequently, the current results cannot establish equivalent risk profiles or identify independent risk-factor associations.

The principal strengths of this study are the restriction to DWI- and ADC-confirmed isolated pontine lesions, blinded independent MRI review by two experienced neurologists, explicit separation of the available topographic dimensions, and the use of statistical procedures suited to sparse categorical data and multiple comparisons.

5. Limitations

Nevertheless, several limitations should guide interpretation of the results. The retrospective single-center design, unconfirmed consecutive enrollment, and small, uneven etiologic and morphological groups increase the risks of selection bias and imprecise estimates. Routine etiologic categories were derived from clinical records, were not assigned independently of lesion topography, and could not be tied to uniform vascular imaging or prolonged rhythm investigations, leaving open the possibility of misclassification. Paired pre-consensus reader ratings were unavailable, preventing the retrospective calculation of inter-rater agreement. Acquisition parameters were available only for representative console exports and may not describe every examination. The dataset also lacked quantitative lesion burden, coordinate-based territory boundaries, exact symptom-onset-to-MRI and symptom-onset-to-NIHSS intervals, serial neurological assessments, and modified Rankin Scale outcomes. Sparse subgroups and missing lesion-burden data precluded reliable multivariable adjustment, meaning that independent anatomical or etiologic effects could not be estimated. Although analytic transparency was strengthened by Monte Carlo exact tests, sensitivity analyses, and control of multiplicity, these cannot overcome the design and data constraints. Consequently, the 69/365 distribution estimate should be read as a record-based hospital proportion rather than as a population prevalence estimate. The hospital proportion is reported without a confidence interval because conventional binomial precision does not account for uncertainty in case ascertainment and record selection.

Within the boundaries of these constraints, our study provides an integrated examination of how routine pontine imaging labels intersect with clinical etiologic classification. Separating lesion side, rostrocaudal segment, and recorded morphology/topography clarifies which patterns are observable and which cannot be interpreted independently. Multicenter prospective studies should use standardized anatomical boundaries, retain independent reader ratings, quantify lesion volume and basal-surface extension, document parent-artery wall findings and rhythm-monitoring completeness, and record serial neurological and functional outcomes. Such studies would help to determine whether the observed patterns are reproducible, and whether specific imaging features add clinically useful information beyond lesion burden and vascular mechanism.

6. Conclusions

In this hospital-based retrospective series of 69 patients, anteromedial morphology and the operational small-vessel/lacunar group were the most frequent recorded categories. The middle pons was the most frequently recorded segment, but allocation of remainder slices to that category may have contributed to its apparent predominance. This finding should not be interpreted as preferential involvement of anatomically equal rostrocaudal thirds. No statistically significant association was detected between rostrocaudal segment and etiologic category.

The apparent associations of lesion side and recorded morphology/topography with etiology in the full cohort were no longer statistically significant after exclusion of the six patients comprising both the bilateral-lesion and large-artery atherosclerosis groups, underscoring the influence of overlapping classifications. Collectively, these findings provide a structured characterization of pontine DWI patterns and their etiologic distribution. Moreover, they support prospective studies incorporating standardized topographic definitions, quantitative lesion assessment, and detailed parent-artery imaging.

Availability of Data and Materials

The de-identified data supporting the findings are not publicly available because of institutional, ethical, and patient-confidentiality restrictions. Subject to institutional approval, de-identified data may be available from the corresponding author upon reasonable request. No data that could directly or indirectly identify patients will be shared.

Author Contributions

MM and FSM designed the research study. MM, BK and FSM developed the methodology. BK and FSM performed the research and curated the data. MM analyzed the data and prepared the visualizations. MM drafted the manuscript. MM and FSM supervised the research. All authors contributed to editorial changes in the manuscript. All authors read and approved the final manuscript. All authors have participated sufficiently in the work and agreed to be accountable for all aspects of the work.

Ethics Approval and Consent to Participate

The study was carried out in accordance with the guidelines of the Declaration of Helsinki and approved by the Ethics Committee of Dr. Burhan Nalbantoğlu State Hospital (Protocol No. YTK.1.01 [EK 41/22]). The requirement for informed consent was waived by the Ethics Committee of Dr. Burhan Nalbantoğlu State Hospital because the study was retrospective. The research was conducted at Dr. Burhan Nalbantoğlu State Hospital, where all clinical data were collected.

Acknowledgment

Not applicable.

Funding

This research received no external funding.

Conflicts of Interest

The authors declare no conflicts of interest.

Declaration of AI and AI-Assisted Technologies in the Writing Process

AI-assisted tools were used to support language editing, document consistency checks, and statistical code review. They did not make clinical diagnoses, independently assign etiologic categories, or interpret diagnostic images. The authors verified the data, clinical classifications, analyses, references, and final text and take full responsibility for the work.

Supplementary Material

Supplementary material associated with this article can be found, in the online version, at https://doi.org/10.31083/RN55179.

References

[1] Bassetti C, Bogousslavsky J, Barth A, Regli F. Isolated infarcts of the pons. Neurology. 1996; 46: 165–175. https://doi.org/10.1212/wnl.46.1.165

[2] Kumral E, Bayülkem G, Evyapan D. Clinical spectrum of pontine infarction. Clinical-MRI correlations. Journal of Neurology. 2002; 249: 1659–1670. https://doi.org/10.1007/s00415-002-0879-x

[3] Kataoka S, Hori A, Shirakawa T, Hirose G. Paramedian pontine infarction. Neurological/topographical correlation. Stroke. 1997; 28: 809–815. https://doi.org/10.1161/01.str.28.4.809

[4] Fisher CM. The arterial lesions underlying lacunes. Acta Neuropathologica. 1968; 12: 1–15. https://doi.org/10.1007/BF00685305

[5] Caplan LR. Intracranial branch atheromatous disease: a neglected, understudied, and underused concept. Neurology. 1989; 39: 1246–1250. https://doi.org/10.1212/wnl.39.9.1246

[6] Erro ME, Gállego J, Herrera M, Bermejo B. Isolated pontine infarcts: etiopathogenic mechanisms. European Journal of Neurology. 2005; 12: 984–988. https://doi.org/10.1111/j.1468-1331.2005.01119.x
[7] Ju Y, Hussain M, Asmaro K, Zhao X, Liu L, Li J, et al. Clinical and imaging characteristics of isolated pontine infarcts: a one-year follow-up study. Neurological Research. 2013; 35: 498–504. https://doi.org/10.1179/1743132813Y.0000000207
[8] Klein IF, Lavallée PC, Mazighi M, Schouman-Claeys E, Labreuche J, Amarenco P. Basilar artery atherosclerotic plaques in paramedian and lacunar pontine infarctions: a high-resolution MRI study. Stroke. 2010; 41: 1405–1409. https://doi.org/10.1161/STROKEAHA.110.583534
[9] Xia C, Chen HS, Wu SW, Xu WH. Etiology of isolated pontine infarctions: a study based on high-resolution MRI and brain small vessel disease scores. BMC Neurology. 2017; 17: 216. https://doi.org/10.1186/s12883-017-0999-7
[10] Kim BJ, Lee KM, Kim HY, Kim YS, Koh SH, Heo SH, et al. Basilar Artery Plaque and Pontine Infarction Location and Vascular Geometry. Journal of Stroke. 2018; 20: 92–98. https://doi.org/10.5853/jos.2017.00829
[11] Feng C, Xu Y, Bai X, Hua T, Li Q, Tang GY, et al. Basilar artery atherosclerosis and hypertensive small vessel disease in isolated pontine infarctions: a study based on high-resolution MRI. European Neurology. 2013; 70: 16–21. https://doi.org/10.1159/000346577
[12] Oh S, Bang OY, Chung CS, Lee KH, Chang WH, Kim GM. Topographic location of acute pontine infarction is associated with the development of progressive motor deficits. Stroke. 2012; 43: 708–713. https://doi.org/10.1161/STROKEAHA.111.632307
[13] Huang R, Zhang X, Chen W, Lin J, Chai Z, Yi X. Stroke Subtypes and Topographic Locations Associated with Neurological Deterioration in Acute Isolated Pontine Infarction. Journal of Stroke and Cerebrovascular Diseases. 2016; 25: 206–213. https://doi.org/10.1016/j.jstrokecerebrovasdis.2015.09.019
[14] Gökçal E, Niftaliyev E, Baran G, Deniz Ç, Asil T. Progressive deficit in isolated pontine infarction: the association with etiological subtype, lesion topography and outcome. Acta Neurologica Belgica. 2017; 117: 649–654. https://doi.org/10.1007/s13760-017-0827-2
[15] Li H, Dai Y, Wu H, Luo L, Wei L, Zhou L, et al. Predictors of Early Neurologic Deterioration in Acute Pontine Infarction. Stroke. 2020; 51: 637–640. https://doi.org/10.1161/STROKEAHA.119.027239
[16] Liu Y, Peng H, Wang J, He L, Xu J, Zheng M, et al. Risk factors for early neurological deterioration in acute isolated pontine infarction without any causative artery stenosis. BMC Neurology. 2022; 22: 332. https://doi.org/10.1186/s12883-022-02861-5
[17] Wang C, Ji J, Wang W, Wang Y. Morphological predictors of neurological deterioration in patients with acute isolated pontine infarct. Acta Neurologica Belgica. 2023; 123: 1371–1379. https://doi.org/10.1007/s13760-023-02234-w
[18] Song X, He F, Hou D, Zhao H, Wei C, Chen L, et al. Imaging biomarker associated with early neurological deterioration in isolated pontine infarction. Frontiers in Neurology. 2024; 15: 1492166. https://doi.org/10.3389/fneur.2024.1492166
[19] von Elm E, Altman DG, Egger M, Pocock SJ, Gøtzsche PC, Vandenbroucke JP, et al. The Strengthening the Reporting of Observational Studies in Epidemiology (STROBE) statement: guidelines for reporting observational studies. Annals of Internal Medicine. 2007; 147: 573–577. https://doi.org/10.7326/0003-4819-147-8-200710160-00010
[20] Brott T, Adams HP, Jr, Olinger CP, Marler JR, Barsan WG, Biller J, et al. Measurements of acute cerebral infarction: a clinical examination scale. Stroke. 1989; 20: 864–870. https://doi.org/10.1161/01.str.20.7.864
[21] Adams HP, Jr, Bendixen BH, Kappelle LJ, Biller J, Love BB, Gordon DL, et al. Classification of subtype of acute ischemic stroke. Definitions for use in a multicenter clinical trial. TOAST. Trial of Org 10172 in Acute Stroke Treatment. Stroke. 1993; 24: 35–41. https://doi.org/10.1161/01.str.24.1.35
[22] Yang H, Liu H, Zhang K, Zong C, Wang A, Wang Y, et al. Neuroimaging markers of early neurological deterioration in acute isolated pontine infarction. Neurological Sciences. 2023; 44: 3607–3614. https://doi.org/10.1007/s10072-023-06837-2
[23] Gao S, Wu W, Yang H, Gou Y. Predictive Factors of Early Neurologic Deterioration in Isolated Pontine Infarction. Annals of Indian Academy of Neurology. 2025; 28: 38–42. https://doi.org/10.4103/aian.aian_883_24
[24] Dell'Acqua B, Vabanesi M, Semerano A, Chieffo R, Giacalone G, Bacigaluppi M, et al. Early deterioration in isolated pontine stroke: predictors and outcomes. Journal of Neurology. 2026; 273: 369. https://doi.org/10.1007/s00415-026-13897-9
[25] Werring DJ, Ozkan H, Doubal F, Dawson J, Freemantle N, Hassan A, et al. Early neurological deterioration in acute lacunar ischemic stroke: Systematic review of incidence, mechanisms, and prospects for treatment. International Journal of Stroke. 2025; 20: 7–20. https://doi.org/10.1177/17474930241273685
[26] Kobayashi J, Ohara T, Minematsu K, Nagatsuka K, Toyoda K. Etiological mechanisms of isolated pontine infarcts based on arterial territory involvement. Journal of the Neurological Sciences. 2014; 339: 113–117. https://doi.org/10.1016/j.jns.2014.01.039
[27] Baran G, Gultekin TO, Baran O, Deniz C, Katar S, Yildiz GB, et al. Association between etiology and lesion site in ischemic brainstem infarcts: a retrospective observational study. Neuropsychiatric Disease and Treatment. 2018; 14: 757–766. https://doi.org/10.2147/NDT.S154224
[28] Huang J, Qiu Z, Zhou P, Li J, Chen Y, Huang R, et al. Topographic location of unisolated pontine infarction. BMC Neurology. 2019; 19: 186. https://doi.org/10.1186/s12883-019-1411-6
[29] Caplan LR. Lacunar infarction and small vessel disease: pathology and pathophysiology. Journal of Stroke. 2015; 17: 2–6. https://doi.org/10.5853/jos.2015.17.1.2
[30] Lim SH, Choi H, Kim HT, Kim J, Heo SH, Chang DI, et al. Basilar plaque on high-resolution MRI predicts progressive motor deficits after pontine infarction. Atherosclerosis. 2015; 240: 278–283. https://doi.org/10.1016/j.atherosclerosis.2015.03.029
[31] Men X, Hu M, Guo Z, Li Y, Zheng L, Wu R, et al. Culprit Plaques of Large Parent Arteries, Rather than Cerebral Small Vessel Disease, Contribute to Early Neurological Deterioration in Stroke Patients with Intracranial Branch Atheromatous Disease. Cerebrovascular Diseases. 2024; 53: 88–97. https://doi.org/10.1159/000530371
[32] Liu HM, Huang A, Wu CH, Huang YC, Hsu LS, Yang N, et al. Detecting Basilar Artery Wall Pathology in Isolated Pontine Infarction With Short-TE SWI Magnitude Images. Stroke: Vascular and Interventional Neurology. 2026; 6: e002131. https://doi.org/10.1161/SVIN.125.002131
[33] Oge DD, Arsava EM, Topcuoglu MA. Basilar Dolichoarteriopathy and Early Clinical Deterioration in Acute Isolated Pontine Infarction. The Neurologist. 2025; 30: 145–149. https://doi.org/10.1097/NRL.0000000000000606
[34] Alemseged F, Rocco A, Arba F, Schwabova JP, Wu T, Cavicchia L, et al. Posterior National Institutes of Health Stroke Scale Improves Prognostic Accuracy in Posterior Circulation Stroke. Stroke. 2022; 53: 1247–1255. https://doi.org/10.1161/STROKEAHA.120.034019
[35] Chai Z, Chen W, Ye Y, Song M, Lin L, Lin D, et al. Intravenous thrombolysis prevents neurological deterioration in patients with acute pontine infarction. Frontiers in Neurology. 2025; 16: 1462372. https://doi.org/10.3389/fneur.2025.1462372